Appendix sections for

A matter of time: Using dynamics and theory to uncover mechanisms of transcriptional bursting

Nicholas C Lammers[1], Yang Joon Kim[1,*], Jiaxi Zhao[2,*], Hernan G Garcia[1,2,3,4,**]

Abstract

Eukaryotic transcription generally occurs in bursts of activity lasting minutes to hours; however, state-of-the-art measurements have revealed that many of the molecular processes that underlie bursting, such as transcription factor binding to DNA, unfold on timescales of seconds. This temporal disconnect lies at the heart of a broader challenge in physical biology of predicting transcriptional outcomes and cellular decision-making from the dynamics of underlying molecular processes. Here, we review how new dynamical information about the processes underlying transcriptional control can be combined with theoretical models that predict not only averaged transcriptional dynamics, but also their variability, to formulate testable hypotheses about the molecular mechanisms underlying transcriptional bursting and control. These We argue that a discourse between theory and experiment that goes beyond understanding averaged will provide a powerful lens for extracting mechanistic insights from live imaging data. will be critical to achieving a predictive understanding of how individual molecular processes combine to generate transcriptional bursting and to facilitate transcriptional control.

Keywords: Live imaging, Transcriptional bursting, Gene regulation, Transcriptional dynamics, Theoretical models of transcription, Non-equilibrium models of transcription, Waiting time distributions

*These authors contributed equally to this work.

**For correspondence: hggarcia@berkeley.edu (HGG)

[1]Biophysics Graduate Group, University of California at Berkeley, Berkeley, California

[2]Department of Physics, University of California at Berkeley, Berkeley, California

[3]Department of Molecular and Cell Biology, University of California at Berkeley, Berkeley, California

[4]Institute for Quantitative Biosciences-QB3, University of California at Berkeley, Berkeley, California

Appendix A. Literature summary of timescales of transcriptional bursting and associated molecular processes

In this section, we present a survey of timescales observed for transcriptional bursting across a broad swath of organisms (Appendix Table A.1). Further, we review *in vivo* and *in vitro* measurements that have revealed the timescales of the molecular transactions underlying transcription and its control.

Recent technological advances such as single-molecule tracking, live-cell imaging, and a variety of high-throughput sequencing methods, have revealed how eukaryotic transcription is driven by a dizzying array of molecular processes that span a wide range of timescales. The overview of these timescales presented in Figure 1E show how many of these processes are significantly faster than transcriptional bursting.

Chromatin accessibility is a central control point for regulating transcription in eukaryotes [1, 2]. DNA wrapped around nucleosome restricts transcription factor access [2, 3]. Multiple studies have determined the timescales of spontaneous DNA unwrapping and rewrapping to be around 0.01-5 s [4–6]. While unwrapping and rewrapping are probably too fast to directly lead to long transcriptional bursts, DNA unwrapping might represent a "foothold" by which factors transiently bind DNA and enact larger-scale, sustained chromatin modifications [2].

Interestingly, nucleosome turnover occurs over a longer timescale compatible with bursting, with multiple studies suggesting timescales of several minutes to hours [7–11]. Recent genome-wide studies have measured average nucleosome turnover time to be approximately 1 hour in the fly and in yeast [7, 8]. Further, histone modifications may modulate nucleosomal occupancy [2, 12, 13], and the half-life as well as addition of these modifications can also span a broad range of timescales compatible with bursting, from several minutes to days [14–20].

Once the chromatin is open, enhancers, DNA stretches containing transcription factor binding sites and capable of contacting promoters to control gene expression, become accessible. Transcription factor binding recruits co-factors and general transcription factors to the promoter, triggering the biochemical cascade that ultimately initiates transcription [21]. While the resulting bursts of RNAP initiation last from a few minutes to hours (Figure 1A-D), single-molecule live imaging has shown that transcription factor binding is a highly transient process, with residence times of 0.5-15 s [22–30]. The vast majority of transcription factors bind DNA for seconds, but it is worth noting that some transcription factors and chromatin proteins can bind DNA for minutes [31, 32].

However, the binding of transcription factors, the general transcriptional machinery, and RNAP to the DNA might be more complex than the simple cartoon picture of individual molecules engaging and disengaging from the DNA. For example, recent experiments have revealed that both mediator and RNAP form transient clusters with relatively short

lifetimes in mammalian nuclei of 5-13 s, 10 s, respectively [33–36]. In addition, it is demonstrated that transcription factors can also form clusters *in vivo* [22, 23]. However, how these cluster dynamics relate to transcriptional activity remains unclear.

Further, enhancers and promoters are often separated by kbp to even Mbp. The mechanism by which enhancers find their target loci from such a large distance, and how this contact triggers transcription, remain uncertain and are reviewed in [37]. *In vivo* measurements of enhancer-promoter separation in the *Drosophila* embryo have shown that this distance fluctuates with a timescale of tens of seconds to several minutes [38–40] —timescales strikingly similar to those of bursting. However, recent work has cast doubt on the simple "lock and key" model of enhancer association (stable, direct contact between enhancers and promoters triggers transcription), suggesting instead that enhancers may activate cognate loci from afar and, in some cases, may activate multiple target loci simultaneously [37, 39–44]. Many important questions remain about the nature of enhancer-driven activation and it remains to be seen whether enhancer association dynamics are generic aspect of eukaryotic transcriptional regulation, or whether they only pertain to a subset of organisms and genes.

A single transcriptional burst generally consists of multiple RNAP initiation events ($\sim$10-100 at a rate of 1/6-1/3 s when the promoter is ON in *Drosophila*, for instance) [45–48]. The transcriptional bursting cycle thus encompasses a smaller, faster biochemical cycle in which RNAP molecules are repeatedly loaded and released by the general transcription machinery. One interesting hypothesis for the molecular origin of transcriptional bursting is that the OFF state between bursts is enacted by an RNAP molecule that becomes paused at the promoter, effectively creating a traffic jam [49]. Live imaging and genome-wide studies have shown that RNAP pausing before initiation is common in eukaryotes [49–52] and that its half-life of up to 20 min can be consistent with transcriptional bursting [53–60].

Although the dynamics of some of the molecular processes outlined above are compatible with the long timescales of transcriptional bursting, we still lack a holistic picture of how these kinetics are integrated to realize transcriptional bursts and, ultimately, to facilitate the regulation of gene expression by transcription factors.

We must also acknowledge that we still lie at the very beginning of a reckoning with the dynamics of transcriptional processes as measurements for some molecular processes results in a range of timescales that are difficult to reconcile. In particular, we still lack solid dynamic measurements regarding the assembly of the transcription preinitiation complex. Yet, perhaps more egregious than the lack of any individual dynamical measurement is the lack of a comprehensive, quantitative, and predictive understanding of how these molecular processes interact with one another in time and space to give rise to transcriptional bursting.

Table A.1: **Literature summary of transcriptional bursting.** We attempted to summarize the duration of a single transcriptional burst from various organisms and genes. In the cases where the single-cell data are not available, such as in data stemming from smFISH experiments, we used population averaged T_{ON} and/or T_{OFF} values instead to give a sense on the timescales.

System	Method	Bursting Timescale	Reference
Bacteria			
in vitro	single-molecule assay	5-8 minutes	[61]
Tet system	MS2	$T_{ON} \approx 6$ minutes, $T_{OFF} \approx 37$ minutes	[62]
Fruit fly embryo			
even-skipped stripe 2	MS2	few minutes	[45, 47]
even-skipped	MS2	few minutes	[63]
Notch signaling	MS2	5-20 minutes	[64]
snail, Krüpple	MS2	5 minutes	[41]
gap genes: *hunchback, giant, Krüpple, knirps*	smFISH	$T_{ON} \approx 3$ minutes, $T_{OFF} \approx 6$ minutes	[65]
hunchback	MS2	few minutes	[66]
even-skipped stripe 2	MS2	few minutes	[47]
Nematode			
Notch signaling	MS2	10-70 minutes	[67]
Human, Mouse			
TGF-β signaling	luciferase assay	few hours	[68]
TFF-1 signaling	MS2	few hours	[69]
liver genes	smFISH	$T_{ON} \approx 30$ minutes - 2 hours	[70]
mammalian genes	luciferase assay	few hours	[71]
Amoeba			
actin gene family	RNA-seq	few hours	[72]
actin gene family	MS2	10-15 minutes	[73]

Table A.2: **Summary of measured timescales of underlying molecular processes associated with transcription.**[5]

System	Organism	Experimental method	Timescale	Reference
Nucleosomal DNA Wrapping/Unwrapping				
Mononucleosomes	*In vitro* reconstitution	FRET	0.1-5 s	[4]
Mononucleosomes	*In vitro* reconstitution	FRET	10-250 ms	[5]
Mononucleosomes	*In vitro* reconstitution	Photochemical crosslinking	<1 s	[6]
Nucleosome Turnover				
Histone H3.3	Fruit fly cell	Genome-wide profiling	1-1.5 h	[7]
Histone H3	Yeast	Genomic tiling arrays	∼1 h	[8]
Histone H2B, H3, and H4 tagged with GFP	Human cell	FRAP	several minutes	[9]
Histone H1 tagged with GFP	Human cell	FRAP	several minutes	[10]
Histone H3	Plant cell	Isotope labeling	several hours	[11]
Histone Modification				
dCas9 inducible recruitment	Mammalian cell	Single-cell imaging	several hours to days	[14]
rTetR inducible recruitment	Mammalian cell	Single-cell imaging	several hours to days	[15]
Chemical-mediated recruitment	Mammalian cell	Chromatin *in vivo* assay	several days	[16]
Histone H3	Human cell	Liquid chromatography, mass spectrometer	several hours to days (half-maximal time of methylation)	[17]
Targeted recruitment	Yeast	ChIP	5-8min (reversal of targeted deacetylation) 1.5 min(reversal of targeted acetylation)	[18]
Histone H2a, H2b, H3, and H4	Mammalian cell	Isotope labeling	<15 min (acetylation half-life)	[19]
Histone H2, H2a and H2b	Mammalian cell	Isotope labeling	∼3 min (acetylation half-life)	[20]

[5]While the vast majority of transcription factors bind DNA for seconds, it is worth noting that some transcription factors (e.g. TATA-binding protein) and chromatin proteins (e.g. CTCF, Cohesin) can bind DNA for minutes. These outliers are not included in Figure 1.

Transcription Factor Binding				
Bicoid	Fruit fly embryo	SMT	∼2 s	[22]
Bicoid	Fruit fly embryo	SMT	∼1 s	[23]
Zelda	Fruit fly embryo	SMT	∼5 s	[22]
Zelda	Fruit fly embryo	FRAP, FCS	∼2-3 s	[24]
Sox2	Mammalian cell	SMT	∼12-15 s	[25]
p53	Mammalian cell	SMT	∼3.5 s	[26]
p53	Mammalian cell	SMT, FRAP, FCS	∼1.8 s	[28]
Glucocorticoid receptor	Mammalian cell	SMT	∼8.1 s	[26]
Glucocorticoid receptor	Mammalian cell	SMT	∼1.45 s	[27]
STAT1	Mammalian cell	SMT	∼0.5 s	[29]
TFIIB	*In vitro* reconstitution	SMT	∼1.5 s	[30]
TATA-binding protein	Mammalian cell	SMT	1.5-2 min	[31]
Chromatin Protein Binding				
CTCF	Mammalian cell	SMT	∼1-2 min	[32]
Cohesin	Mammalian cell	SMT	∼22 min	[32]
RNAP Cluster Dynamics				
RNAP tagged with Dendra2	Mammalian cell	tcPALM	∼12.9 s (with small fraction of stable clusters)	[33]
RNAP tagged with Dendra2	Mammalian cell	tcPALM	∼8.1 s	[34]
RNAP tagged with Dendra2	Human cell	Bayesian nanoscopy	several seconds	[35]
RNAP tagged with Dendra2	Human cell	tcPALM	∼5.1 s	[36]
Mediator Cluster Dynamics				
Mediator tagged with Dendra2	Mammalian cell	tcPALM	∼11.1 s	[33]
Enhancer-Promoter Interaction				
snail shadow enhancer	Fruit fly embryo	MS2, PP7 labeling	∼10-40 s (fluctuation cycle interval)	[38]
snail enhancer	Fruit fly embryo	MS2, PP7 labeling	several minutes	[39]
endogenous *even-skipped* locus with homie insulator	Fruit fly embryo	MS2, PP7 labeling	several minutes	[40]

Transcription Initiation				
even-skipped stripe 2 enhancer	Fruit fly embryo	MS2 labeling	∼3 s (promoter ON)	[45]
HIV-1 promoter	Mammalian cell	MS2 labeling	∼4.1 s (promoter ON)	[46]
hb P2 enhancer	Fruit fly embryo	MS2 labeling	∼6 s	[48]
Promoter-Proximal Pausing				
RNAP tagged with GFP	Human cell	FRAP	∼40 s	[53]
RNAP (genome-wide)	Fruit fly cell	RNA sequencing	∼2-20 min	[54]
RNAP (genome-wide)	Fruit fly cell	ChIP-nexus	∼5-20 min	[55]
RNAP (genome-wide)	Fruit fly cell	Genome-wide footprinting	∼2.5-20 min	[56]
RNAP tagged with GFP	Fruit fly salivary glands	Single-cell imaging	∼5 min	[57]
RNAP (genome-wide)	Mammalian cell	GRO-seq	∼6.9 min (average)	[58]
RNAP (genome-wide)	Fruit fly cell	scRNA-seq	15-20 min (at genes with low activity)	[59]
LacO-tagged minimal CMV promoter	Human cell	MS2 labeling, FRAP	∼4 min	[60]

SMT: Single-molecule tracking

FRAP: Fluorescence recovery after photobleaching

FCS: Fluorescence correlation spectroscopy

FRET: Fluorescence resonance energy transfer

ChIP: Chromatin immunoprecipitation

PALM: Photo-activated localization microscopy

Appendix B. Two-state model calculations

As noted in the main text, the average initiation rate is equal to r times the average fraction of time the promoter spends in this ON state p_{on},

$$\left\langle \text{initiation rate} \right\rangle = r\, p_{on}. \tag{B.1}$$

To predict the effect of bursting on transcription initiation, it is necessary to determine how p_{on} depends on the bursting parameters. In the mathematical realization of the two-state model shown in Figure 2A, the temporal evolution of p_{off}, the average probability of being in the OFF state, and of p_{on} is given by

$$\frac{dp_{off}}{dt} = -k_{on}\, p_{off} + k_{off}\, p_{on}, \tag{B.2}$$

and

$$\frac{dp_{on}}{dt} = k_{on}\, p_{off} - k_{off}\, p_{on}. \tag{B.3}$$

To solve these equations, we make the simplifying assumption that our system is in steady state such that these average probabilities of finding the system on the ON and OFF states are constant in time. In this scenario, we can set the rates dp_{off}/dt and dp_{on}/dt to zero. We then solve for k_{off} in terms of k_{on} resulting in

$$k_{off} = \frac{k_{on}\, p_{off}}{p_{on}}. \tag{B.4}$$

Plugging in the normalization condition $p_{on} + p_{off} = 1$ gives us

$$k_{off} = \frac{k_{on}\,(1 - p_{on})}{p_{on}}, \tag{B.5}$$

which can be solved in terms of k_{on}, k_{off}, resulting in

$$p_{on} = \frac{k_{on}}{k_{on} + k_{off}}. \tag{B.6}$$

Appendix C. Molecular model calculations

Here we provide a brief overview of the calculations relating to the three theoretical models of transcription presented in Section 3: the independent binding model (Figure 3C), the cooperative binding model (Figure 3E) and the rate-limiting step model (Figure 3G). We also provide resources relating to the calculation of first-passage time distributions discussed in section 4.

Appendix C.1. Stochastic simulations

We make heavy use of stochastic simulations throughout this work. A custom-written implementation of the Gillespie Algorithm [74] was used to simulate trajectories for the various models discussed in the main text. These simulated trajectories were used to generate the activity trace plots in Figure 3D, F, and G, as well as the first-passage time distributions in Figure 4B-D. All code related to this project (including the Gillespie Algorithm implementation for stochastic activity trace generation) can be accessed on GitHub [75].

Appendix C.2. Independent binding model

All calculations in this section pertain to the independent binding model presented in Figure 3C.

Appendix C.2.1. Calculating state probabilities

Calculating the probability of each activity state is central to determining a system's overall transcriptional behavior. Because our mathematical model is a linear chain with no cycles (see Figure 3B), we can make progress towards calculating the steady state probabilities, p_i, by imposing detailed balance, which gives

$$p_n k_+(n) = p_{n+1} k_-(n+1), \tag{C.1}$$

where k_+ and k_- are the effective rates of adding and subtracting a single activator molecule that we define in Figure 3B. Plugging in Equation C.34 and Equation 6 from the main text results in

$$p_n(N-n)k_{n,n+1} = p_{n+1}(n+1)k_{n+1,n}, \tag{C.2}$$

where, the rates $k_{n,n+1}$ and $k_{n+1,n}$ are the microscopic binding and unbinding rates defined in Figure 3A, respectively. Now we make use of the fact that there are only two unique microscopic rates in the independent binding system: activator molecules bind at a rate $k_{n,n+1} = k^b = k_0^b[A]$, with $[A]$ being the activator concentration and k_0^b the binding rate constant, and unbind at a rate $k_{n,n-1} = k^u$. Plugging these values into Equation C.2 and rearranging leads to

$$p_{n+1} = \Big(\frac{N-n}{n+1}\Big)\Big(\frac{k^b}{k^u}\Big)p_n. \tag{C.3}$$

To further simplify the expression in Equation C.3, we write $\frac{k^u}{k^b}$ as a dissociation constant (K_d), resulting in

$$p_{n+1} = \Big(\frac{N-n}{n+1}\Big)\frac{p_n}{K_d}, \tag{C.4}$$

which has the form of a recursive formula for calculating state probabilities from their predecessors. For instance, for the case where $n = 0$ we have

$$p_1 = N\frac{p_0}{K_d}. \tag{C.5}$$

We can extend this logic to calculate the probability of any state, n, as a function of p_0, leading to

$$p_n = \frac{N!}{(N-n)!n!}\frac{p_0}{K_d^n} = \binom{N}{n}\frac{p_0}{K_d^n}, \tag{C.6}$$

where we have replaced the factorial terms with the binomial coefficient ($\binom{N}{n}$) on the far right-hand side can be thought of as accounting for the fact that a given number of activators bound, n, may correspond to multiple microscopic binding configurations (compare Figure 3A and B). Note that $\binom{N}{0} = 1$, which means that Equation C.6 is valid even when $n = 0$. Finally, we impose the normalization condition that the sum of the state probabilities should be equal to 1, which leads to

$$p_n = \frac{p_0\binom{N}{n}K_d^{-n}}{p_0\sum_{i=0}^{N}\binom{N}{i}K_d^{-i}}. \tag{C.7}$$

Canceling out the factors of p_0 gives us our final expression for p_n, namely

$$p_n = \frac{\binom{N}{n}K_d^{-n}}{\sum_{i=0}^{N}\binom{N}{i}K_d^{-i}} = \frac{\binom{N}{n}K_d^{-n}}{Z}, \tag{C.8}$$

where Z on the far righ-hand side indicates the sum of all state weights. Thus, given values of the rates k^b and k^u, which define K_d, we can calculate the probability of the system being in each binding state n. This probability is shown diagrammatically in the shading of the different states in Figure 3C.

Appendix C.2.2. Independent binding cannot produce bimodal transcriptional output

A basic requirement for bimodal transcriptionl behavior is that $p_0 > p_1$ and $p_N > p_{N-1}$, where N is the total number of binding sites. Couching this in terms of Equation C.8 leads to

$$\frac{p_0}{p_1} = \frac{1}{N}K_d > 1, \tag{C.9}$$

which simplifies to

$$K_d > N \tag{C.10}$$

for the low activity regime and

$$\frac{p_N}{p_{N-1}} = \frac{1}{N}\frac{1}{K_d} > 1, \tag{C.11}$$

leading to

$$K_d < \frac{1}{N} \tag{C.12}$$

for the high activity regime. Since K_d is set by the ratio $\frac{k^u}{k^b}$, which is constant for all states in the independent binding model, it is not possible for it to be simultaneously larger (Equation C.10) and smaller (Equation C.12) than the number of binding sites N. We thus conclude that independent binding is incompatible with bimodal transcription, regardless of the number of binding sites N.

Appendix C.2.3. Diffusion-limited binding

In the main text we state that we set $k^b = [A]k_0^b$ to 0.5 s^{-1} for the simulations shown in Figure 3C. This is convenient because it leads to a model where half the available sites are bound, on average. This choice is also physically reasonable. Bicoid concentrations in the anterior region of the embryo (where *hunchback* is expressed) are on the order of 30 molecules per μm^3 [76]. A k^b of 0.5 s^{-1} thus implies that $k_0^b \approx 0.017$ $\mu\text{m}^3\text{s}^{-1}$ per molecule. This falls below a recent estimate for the upper limit on k_0^b for Bicoid binding set by diffusion of ~ 0.022 $\mu\text{m}^3\text{s}^{-1}$ per molecule [77].

We also note here that the largest binding rate in the cooperative binding model (Figure 3E and F), $k^b = 58$ s^{-1}, implies a k_0^b that is significantly above diffusion limit diffusion limit for Bicoid estimated in [77]. This high binding rate implies that cooperative binding interactions somehow facilitate the super-diffusive recruitment of additional activator molecules to the gene locus. While speculative, we note that the relatively small energies needed to realized this rapid recruitment in our model (for the plots in Figure 3, the cooperativity factor ω equals 6.7, which corresponds to protein-protein interactions with energies of $1.9k_bT$), suggest that this kind of behavior is at least physically plausible. Alternatively, a significant increase in the concentration of activator molecules in the direct vicinity of the gene locus could facilitate rapid activator binding without exceeding the limits set by diffusion. Recent experiments provide evidence for this kind of local enrichment [22, 24], but it remains to be seen whether this phenomenon plays a role in facilitating gene regulation and, in particular, whether local transcription factor enrichment influences bursting.

Finally, we also note that the rate-limiting step model (Figure 3G and H) assumes a binding rate in the ON state, $k_{on}^b = 21$ s^{-1}, that likewise implies a k_0^b that is above Bicoid's likely diffusion limit. This high binding rate was employed primarily

for clarity of exposition, ensuring that the rate-limiting steps separated "ON" and "OFF" activity regimes that were well resolved from one another. Our principal conclusions do not depend on the precise value of k^b_{on}, though, naturally, inferring the durations of OFF (and ON) periods as was done for the waiting time analyses in Figure 4 becomes more difficult. Specifically, smaller values of k^b_{on} reduce the average number of molecules bound when the system is in the ON state,

$$\langle n_{on} \rangle = N \frac{k^b_{on}}{k^b_{on} + k^u_{on}}, \tag{C.13}$$

which leads to more overlap between the transcriptional activity corresponding to the ON and OFF states. It is plausible that a k^b_{on} of this magnitude could be realized by other activator molecules that (i) diffuse faster than Bicoid, (ii) have larger binding target regions, or (iii) are expressed at higher concentrations endogenously. Alternatively, Equation C.13 indicates that a rate-limiting step mechanism that alters the rate of unbinding (k^u) when switching between ON and OFF states instead of, or in conjunction with, k^b could lead to similarly well-resolved ON and OFF states to those in Figure 3H at much lower values of k^b.

Appendix C.3. Cooperative binding

All calculations in this section pertain to the independent binding model presented in Figure 3E.

Appendix C.3.1. Deriving state probabilities with cooperative binding

In Equation 7 of the main text we incorporated cooperativity to binding by adding multiplicative weights, ω, giving

$$k_{i,i+1} = k^b \omega^i. \tag{C.14}$$

This functional form follows from the assumption that each bound activator increases k^b by a constant factor $\omega \geq 1$. This leads the expression for $k_+(n)$

$$k^{coop}_+(n) = (N - n)\omega^n k^b, \tag{C.15}$$

which is a nonlinear function of n. Now, in analogy to the calculations presented in Appendix C.2.1, let's re-derive our expressions for p_n. To start, we have

$$p_{n+1} = \Big(\frac{N-n}{n+1}\Big)\Big(\frac{k^b}{k^u}\Big)\omega^n p_n. \tag{C.16}$$

Again expressing $\frac{k^u}{k^b}$ as a dissociation constant (K_d), we obtain

$$p_{n+1} = \left(\frac{N-n}{n+1}\right)\frac{\omega^n p_n}{K_d}. \tag{C.17}$$

We can also extend this logic to calculate the probability of any state, n, as a function of p_0, leading to

$$p_n = \frac{N!}{(N-n)!n!}\frac{\omega^{\frac{n(n-1)}{2}}p_0}{K_d^n} = \binom{N}{n}\frac{\omega^{\frac{n(n-1)}{2}}p_0}{K_d^n}. \tag{C.18}$$

Finally, by requiring that all state probabilities sum to one, we obtain

$$p_n = \frac{\binom{N}{n}\omega^{\frac{n(n-1)}{2}}K_d^{-n}}{Z}, \tag{C.19}$$

where Z again denotes the sum of all state weights as in Equation C.8. We have used these expressions to calculate the probability of each state shown using the shading in Figure 3E.

Appendix C.3.2. Cooperativity permits bimodal expression

Now, let's use Equation C.18 to examine how the addition of the cooperativity factor ω makes bimodal bursting possible. Recall that bimodal gene expression requires that $p_0 > p_1$ and $p_N > p_{N-1}$. For the low activity regime, cooperativity is not relevant because there are no already bound activators, and so the form of the requirement remains the same, namely

$$\frac{p_0}{p_1} = \frac{1}{N}K_d > 1. \tag{C.20}$$

However, things change in the high activity regime. Here, we have

$$\frac{p_N}{p_{N-1}} = \frac{1}{N}\frac{\omega^{N-1}}{K_d} > 1. \tag{C.21}$$

In stark contrast to the independent binding case, we see that the addition of ω makes it possible to realize both conditions simultaneously, opening the door to bimodal burst behaviors. Specifically, bimodality demands

$$K_d > N, \tag{C.22}$$

and

$$\omega > (NK_d)^{\frac{1}{N-1}} \tag{C.23}$$

to be true.

These requirements thus demonstrate that cooperativity is required to achieve bimodal bursting in the context of this binding model. Indeed, the cooperative binding system shown in Figure 3E and F meets these criteria, having $K_d = 116$ and $\omega = 6.7$, both of which are comfortably above the lower bounds described above for a system with six binding sites ($N = 6$).

Appendix C.3.3. Cooperativity is necessary to simultaneously achieve kinetic trapping at both ends of the chain

In the main text we introduced the concept of "kinetic trapping"; a phenomenon in which large imbalances between between $k_+(n)$ and $k_-(n)$ cause a system to get trapped in high and low activity states for periods of time that far exceed the timescale of individual binding/unbinding events. Here, we show that cooperativity ($\omega > 1$) is needed in order to achieve this kind of trapping at *both* the high and low ends of the binding chain shown in Figure 3B simultaneously.

To begin, we note that the relations $k_-(1) > k_+(1)$ and $k_-(N-1) < k_+(N-1)$ are necessary to have traps at the low and high ends of the chain, respectively. Thus both conditions must hold simultaneously for traps to exist at the low and high ends simultaneously. We can use Equation C.15 and Equation 6 to express these requirements in terms of system parameters. For the low activity regime, we have

$$\frac{k_-(1)}{k_+(1)} = \frac{K_d}{(N-1)\omega} > 1, \tag{C.24}$$

and for the higher regime we obtain

$$\frac{k_+(N-1)}{k_-(N-1)} = \frac{\omega^{N-1}}{(N-1)K^d} > 1. \tag{C.25}$$

We can simplify these requirements to obtain upper and lower bounds on ω, namely

$$\Big[K_d(N-1)\Big]^{\frac{1}{N-1}} \;<\; \omega \;<\; \frac{K_d}{N-1}. \tag{C.26}$$

We see that Equation C.26 implies restrictions on the relationship between K_d and N. Specifically, there must be a gap between the upper and lower bounds in Equation C.26 such that there exist viable ω values. This means that

$$\Big[K_d(N-1)\Big]^{\frac{1}{N-1}} \;<\; \frac{K_d}{N-1}, \tag{C.27}$$

must hold. Upon simplification, this gives

$$(N-1)^N \ < \ K_d^{N-2}. \tag{C.28}$$

$$(N-1)^2 < K_d. \tag{C.29}$$

Equation C.29 tells us that the dissociation constant must be larger than one (indeed, it must be larger than 25 for an $N = 6$ binding site system). This implies that the expression for the lower ω bound on the left-hand side of Equation C.26 is guaranteed to be greater than one as well because

$$K_d(N-1) \ > 1, \tag{C.30}$$

and therefore

$$1 \ < \ \Big[K_d(N-1)\Big]^{\frac{1}{N-1}} \ < \ \omega. \tag{C.31}$$

This indicates that cooperative interactions are necessary to realize kinetic traps on both ends of the chain, though it hints at the fact that increasing the number of binding sites, N, should enable trapping with lower values of ω.

Appendix C.3.4. Off rate-mediated cooperativity can also generate transcriptional bursting

It is straight-forward to adapt our discussion of on rate-mediated cooperativity to capture the case where cooperative interactions act instead to stabilize bound factors and thereby reduce the effective off rate. Indeed, the expressions are identical save for the fact that the basal binding rate is *divided* by powers of ω, rather than multiplied. Namely,

$$k_{i,i-1} = \frac{k^u}{\omega^i}. \tag{C.32}$$

This leads the expression for $k_-(n)$

$$k_-^{coop}(n) = n\frac{k^u}{\omega^n}. \tag{C.33}$$

Since activator binding is assumed to be independent, the expression for $k_+(n)$ is identical to that for the independent binding model, namely,

$$k_+(n) = (N-n)k_{n,n+1}. \tag{C.34}$$

These expressions lead to a model wherein the unbinding rate decreases significantly as more and more activators become bound (Figure C.5A). From this point

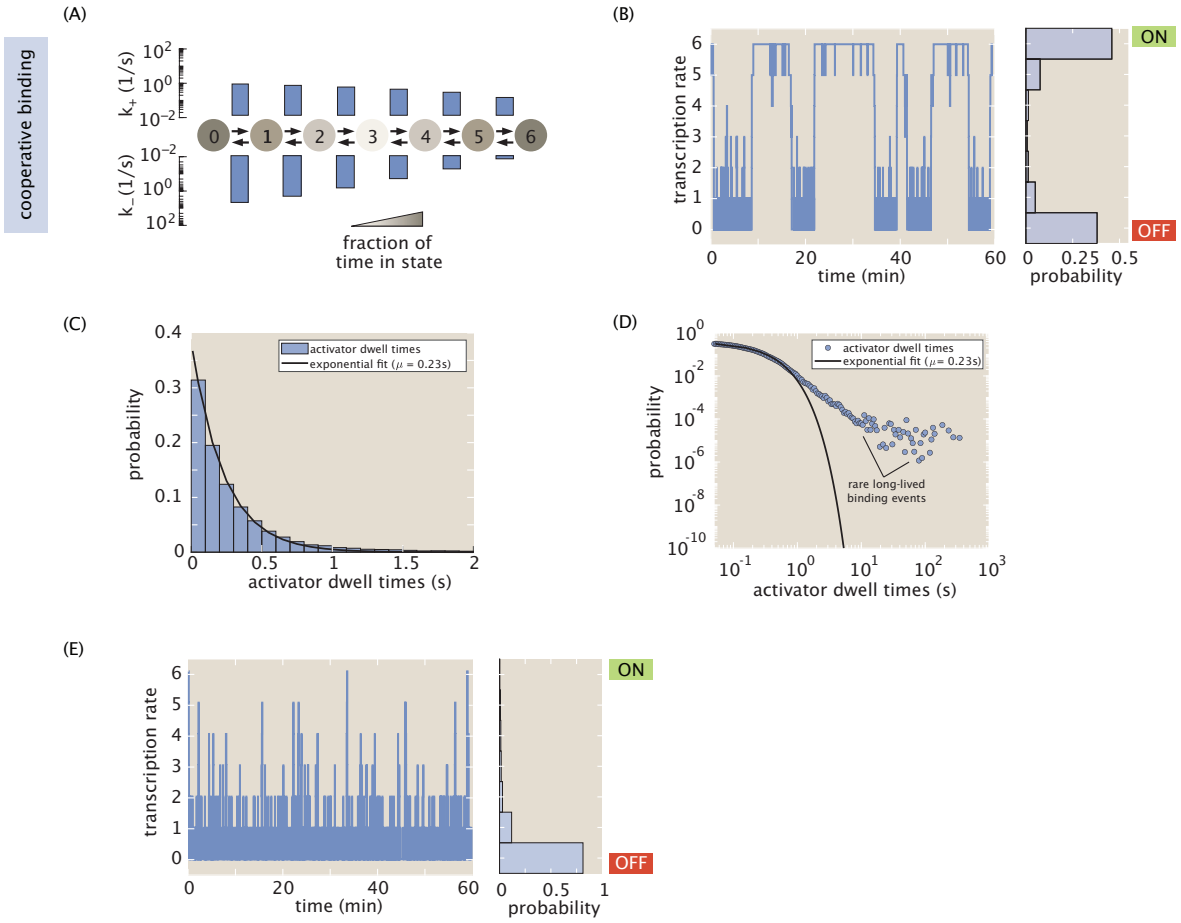

Figure C.5: **Cooperative binding model with off rate-mediated cooperativity**. **(A)** Cooperative binding model in which stabilizing interactions between bound activators decreases the unbinding rate. **(B)** Simulation reveals that off rate-mediated cooperativity can cause the system to exhibit bimodal rates of transcription and slow fluctuations between effective ON and OFF states that are comparable to those observed for on rate-mediated cooperativity (Figure 3E and F). **(C)** The predicted distribution of unbinding times is well fit by a single exponential, despite the presence of cooperative interactions. **(D)** However, this fit masks the presence of rare long-lived binding events that are signatures of the cooperative effects that enable slow timescale bursting. These events can be seen as a significant deviation between the empirical distribution of dwell times (blue circles) from the exponential fit when we shift to looking at the data on a log-log scale. **(E)** To examine the role these long-lived events play in bursting, we conducted simulations in which all activator dwell events were capped to a maximum duration of 10 seconds; i.e. we forced all activators still bound after 10 seconds to unbind. These simulations revealed that removing long-lived binding events abolishes all burst-like activity.

forward, the expressions for state probabilities (starting with Equation C.16) have precisely the same form as those for the on rate-mediated case.

With the off rate-mediated model thus defined, we are in a position to once again employ stochastic simulations to explore the impact of cooperativity on transcriptional dynamics. These reveal that stabilizing cooperative interactions amongst bound activator molecules can also generate slow bimodal transcriptional fluctuations (Figure C.5B). While this is perhaps not surprising given the close mathematical parallels between the on and off rate-mediated cooperativity models, this result emphasizes the bredth of potential molecular mechanisms that could lead to transcriptional bursting.

Given these results, it is interesting to ask whether stabilizing cooperative interactions should have a clear signature in experimental measurements of individual activator residence times. Somewhat surprisingly, a distribution of single particle unbinding events generated via stochastic simulations are well described by a single exponential fit with a mean residence time of 0.23 s^{-1} (Figure C.5C), which is on the same scale as the empirical measurements in [22]. Yet, this is no the full story. A close inspection of the distribution of dwell times reveals a small ($\lesssim 5\%$) fraction of very long lived binding events that last for 10s to 100s of seconds (Figure C.5D).

Such events might very well be missed in an *in vivo* experiment due either to how rare they are or to limitations on observation time imposed by the bleaching of fluorescent proteins. To examine the role these events play in dictating burst dynamics, we conducted simulations invoking parameters identical to those used to generate the trace shown in Figure C.5B, with one important alteration: all activators still bound after 10 seconds were forced to unbind. This effectively capped the activator dwell time at 10 seconds, thereby abolishing all long-lived binding events. Figure C.5E shows the result of this exercise, clearly indicating, that removing rare long-lived binding events abolishes burst-like dynamics. These results thus indicate that hard-to-detect long-lived binding events could play a key role in generating slow burst dynamics, suggesting that it could be of interest to design experiments explicitly aimed at searching for long-lived binding events *in vivo*. In closing, we note that similar results relating to activator dwell time distributions in the presence of cooperative interactions are discussed in [77]. We direct readers to this work for an excellent, detailed discussion on this topic.

Appendix C.4. First-passage time calculations

In this review we used stochastic simulations (briefly outlined in Appendix C.1) to arrive at expectations for the form of first-passage time distributions for the cooperative binding and rate-limiting step models. All relevant scripts are available

at GitHub. We also note that the functional forms for waiting time distributions can be calculated using analytical methods such as Laplace Transforms. We do not provide the details for this approach here, but point the reader to [78, 79], as well as the sources cited therein, for more information.

References

1. Eck, E. *et al.* Quantitative dissection of transcription in development yields evidence for transcription factor-driven chromatin accessibility. *bioRxiv,* 2020.01.27.922054 (2020).
2. Bowman, G. D. & Poirier, M. G. Post-translational modifications of histones that influence nucleosome dynamics. *Chemical Reviews* **115,** 2274–2295 (2015).
3. Kouzarides, T. Chromatin modifications and their function. *Cell* **128,** 693–705 (2007).
4. Tomschik, M., Zheng, H., Van Holde, K., Zlatanova, J. & Leuba, S. H. Fast long-range, reversible conformational fluctuations in nucleosomes revealed by single-pair fluorescence resonance energy transfer. *Proceedings of the National Academy of Sciences of the United States of America* **102,** 3278–3283 (2005).
5. Li, G., Levitus, M., Bustamante, C. & Widom, J. Rapid spontaneous accessibility of nucleosomal DNA. *Nature Structural and Molecular Biology* **12,** 46–53 (2005).
6. Kassabov, S. R., Zhang, B., Persinger, J. & Bartholomew, B. SWI/SNF unwraps, slides, and rewraps the nucleosome. *Molecular Cell* **11,** 391–403 (2003).
7. Deal, R. B., Henikoff, J. G. & Henikoff, S. Genome-wide kinetics of nucleosome turnover determined by metabolic labeling of histones. *Science* **328,** 1161–1165 (2010).
8. Ghuysen, J. M. *et al.* Dynamics of replication-independent Histone turnover in budding yeast. *Science* **315,** 1405–1409 (2007).
9. Kimura, H. & Cook, P. R. Kinetics of core histones in living human cells: Little exchange of H3 and H4 and some rapid exchange of H2B. *Journal of Cell Biology* **153,** 1341–1353 (2001).
10. Misteli, T., Gunjan, A., Hock, R., Bustin, M. & Brown, D. T. Dynamic binding of histone H1 to chromatin in living cells. *Nature* **408,** 877–881 (2000).
11. Waterborg, J. H. Histone synthesis and turnover in alfalfa. Fast loss of highly acetylated replacement histone variant H3.2. *Journal of Biological Chemistry* **268,** 4912–4917 (1993).

12. Ludwig, C. H. & Bintu, L. Mapping chromatin modifications at the single cell level. *Development* **146** (2019).

13. Lawrence, M., Daujat, S. & Schneider, R. Lateral thinking: How Histone modifications regulate gene expression. *Trends in Genetics* **32,** 42–56 (2016).

14. Braun, S. M. *et al.* Rapid and reversible epigenome editing by endogenous chromatin regulators. *Nature Communications* **8** (2017).

15. Bintu, L. *et al.* Dynamics of epigenetic regulation at the single-cell level. *Science* **351,** 720–724 (2016).

16. Hathaway, N. A. *et al.* Dynamics and memory of heterochromatin in living cells. *Cell* **149,** 1447–1460 (2012).

17. Zee, B. M. *et al.* In vivo residue-specific histone methylation dynamics. *Journal of Biological Chemistry* **285,** 3341–3350 (2010).

18. Katan-Khaykovich, Y. & Struhl, K. Dynamics of global histone acetylation and deacetylation in vivo: Rapid restoration of normal histone acetylation status upon removal of activators and repressors. *Genes and Development* **16,** 743–752 (2002).

19. Chestier, A. & Yaniv, M. Rapid turnover of acetyl groups in the four core histones of simian virus 40 minichromosomes. *Proceedings of the National Academy of Sciences of the United States of America* **76,** 46–50 (1979).

20. Jackson, V., Shires, A., Chalkley, R. & Granner, D. K. Studies on highly metabolically active acetylation and phosphorylation of histones. *Journal of Biological Chemistry* **250,** 4856–4863 (1975).

21. Coulon, A., Chow, C. C., Singer, R. H. & Larson, D. R. Eukaryotic transcriptional dynamics: From single molecules to cell populations. *Nature Reviews Genetics* **14,** 572–584 (2013).

22. Mir, M. *et al.* Dynamic multifactor hubs interact transiently with sites of active transcription in drosophila embryos. *eLife* **7,** 1–27 (2018).

23. Mir, M. *et al.* Dense bicoid hubs accentuate binding along the morphogen gradient. *Genes and Development* **31,** 1784–1794 (2017).

24. Dufourt, J. *et al.* Temporal control of gene expression by the pioneer factor Zelda through transient interactions in hubs. *Nature Communications* **9** (2018).

25. Chen, J. *et al.* Single-molecule dynamics of enhanceosome assembly in embryonic stem cells. *Cell* **156,** 1274–1285 (2014).

26. Morisaki, T., Müller, W. G., Golob, N., Mazza, D. & McNally, J. G. Single-molecule analysis of transcription factor binding at transcription sites in live cells. *Nature Communications* **5** (2014).

27. Gebhardt, J. C. M. *et al.* Single-molecule imaging of transcription factor binding to DNA in live mammalian cells. *Nature Methods* **10** (2013).

28. Mazza, D., Abernathy, A., Golob, N., Morisaki, T. & McNally, J. G. A benchmark for chromatin binding measurements in live cells. *Nucleic Acids Research* **40** (2012).

29. Speil, J. *et al.* Activated STAT1 transcription factors conduct distinct saltatory movements in the cell nucleus. *Biophysical Journal* **101,** 2592–2600 (2011).

30. Zhang, Z. *et al.* Rapid dynamics of general transcription factor TFIIB binding during preinitiation complex assembly revealed by single-molecule analysis. *Genes & development* **30,** 2106–2118 (2016).

31. Teves, S. S. *et al.* A stable mode of bookmarking by TBP recruits RNA polymerase II to mitotic chromosomes. *eLife* **7,** e35621 (2018).

32. Hansen, A. S., Pustova, I., Cattoglio, C., Tjian, R. & Darzacq, X. CTCF and cohesin regulate chromatin loop stability with distinct dynamics. *eLife* **6,** e25776 (2017).

33. Cho, W. K. *et al.* Mediator and RNA polymerase II clusters associate in transcription-dependent condensates. *Science* **361,** 412–415 (2018).

34. Cho, W.-K. *et al.* RNA Polymerase II cluster dynamics predict mRNA output in living cells. *eLife* **5,** e13617 (2016).

35. Chen, X. *et al.* Study of RNA Polymerase II clustering inside live-cell nuclei using Bayesian Nanoscopy. *ACS Nano* **10,** 2447–2454 (2016).

36. Cisse, I. I. *et al.* Real-time dynamics of RNA polymerase II clustering in live human cells. *Science* **341,** 664–667 (2013).

37. Furlong, E. E. & Levine, M. Developmental enhancers and chromosome topology. *Science* **361,** 1341–1345 (2018).

38. Heist, T., Fukaya, T. & Levine, M. Large distances separate coregulated genes in living Drosophila embryos. *Proceedings of the National Academy of Sciences of the United States of America* **116,** 15062–15067 (2019).

39. Lim, B., Heist, T., Levine, M. & Fukaya, T. Visualization of transvection in living Drosophila embryos. *Molecular Cell* **70,** 287–296.e6 (2018).

40. Chen, H. *et al.* Dynamic interplay between enhancer–promoter topology and gene activity. *Nature Genetics* **50,** 1296–1303 (2018).

41. Fukaya, T., Lim, B. & Levine, M. Enhancer control of transcriptional bursting. *Cell* **166,** 358–368 (2016).

42. Gu, B. *et al.* Transcription-coupled changes in nuclear mobility of mammalian cis-regulatory elements. *Science* **359,** 1050–1055 (2018).

43. Benabdallah, N. S. *et al.* Decreased enhancer-promoter proximity accompanying enhancer activation. *Molecular Cell* **76,** 473–484.e7 (2019).

44. Schoenfelder, S. & Fraser, P. Long-range enhancer–promoter contacts in gene expression control. *Nature Reviews Genetics* **20,** 437–455 (2019).

45. Lammers, N. C. *et al.* Multimodal transcriptional control of pattern formation in embryonic development. *Proceedings of the National Academy of Sciences of the United States of America* **117,** 836–847 (2020).

46. Tantale, K. *et al.* A single-molecule view of transcription reveals convoys of RNA polymerases and multi-scale bursting. *Nature Communications* **7,** 12248 (2016).

47. Bothma, J. P. *et al.* Dynamic regulation of eve stripe 2 expression reveals transcriptional bursts in living Drosophila embryos. *Proceedings of the National Academy of Sciences of the United States of America* **111,** 10598–10603 (2014).

48. Garcia, H. G., Tikhonov, M., Lin, A. & Gregor, T. Quantitative imaging of transcription in living Drosophila embryos links polymerase activity to patterning. *Current Biology* **23,** 2140–2145 (2013).

49. Jonkers, I. & Lis, J. T. Getting up to speed with transcription elongation by RNA polymerase II. *Nature Reviews Molecular Cell Biology* **16,** 167–177 (2015).

50. Bartman, C. R. *et al.* Transcriptional burst initiation and Polymerase pause release are key control points of transcriptional regulation. *Molecular Cell* **73,** 519–532.e4 (2019).

51. Gaertner, B. & Zeitlinger, J. RNA polymerase II pausing during development. *Development* **141,** 1179–1183 (2014).

52. Core, L. J., Waterfall, J. J. & Lis, J. T. Nascent RNA sequencing reveals widespread pausing and divergent initiation at human promoters. *Science* **322,** 1845–1848 (2008).

53. Steurer, B. *et al.* Live-cell analysis of endogenous GFP-RPB1 uncovers rapid turnover of initiating and promoter-paused RNA Polymerase II. *Proceedings of the National Academy of Sciences of the United States of America* **115,** E4368–E4376 (2018).

54. Henriques, T. *et al.* Widespread transcriptional pausing and elongation control at enhancers. *Genes & Development* **32,** 26–41 (2018).

55. Shao, W. & Zeitlinger, J. Paused RNA Polymerase II inhibits new transcriptional initiation. *Nature Genetics* **49,** 1045–1051 (2017).

56. Krebs, A. R. *et al.* Genome-wide single-molecule footprinting reveals high RNA Polymerase II turnover at paused promoters. *Molecular Cell* **67,** 411–422.e4 (2017).

57. Buckley, M. S., Kwak, H., Zipfel, W. R. & Lis, J. T. Kinetics of promoter Pol II on Hsp70 reveal stable pausing and key insights into its regulation. *Genes & Development* **28,** 14–19 (2014).

58. Jonkers, I., Kwak, H. & Lis, J. T. Genome-wide dynamics of Pol II elongation and its interplay with promoter proximal pausing, chromatin, and exons. *eLife* **3,** e02407 (2014).

59. Henriques, T. *et al.* Stable pausing by RNA Polymerase II provides an opportunity to target and integrate regulatory signals. *Molecular Cell* **52,** 517–528 (2013).

60. Darzacq, X. *et al.* In vivo dynamics of RNA Polymerase II transcription. *Nature Structural and Molecular Biology* **14,** 796–806 (2007).

61. Chong, S., Chen, C., Ge, H. & Xie, X. S. Mechanism of transcriptional bursting in bacteria. *Cell* **158,** 314–326 (2014).

62. Golding, I., Paulsson, J., Zawilski, S. M. & Cox, E. C. Real-time kinetics of gene activity in individual bacteria. *Cell* **123,** 1025–1036 (2005).

63. Berrocal, A., Lammers, N., Garcia, H. G. & Eisen, M. B. Kinetic sculpting of the seven stripes of the Drosophila even-skipped gene. *bioRxiv,* 335901 (2020).

64. Falo-Sanjuan, J., Lammers, N. C., Garcia, H. G. & Bray, S. J. Enhancer priming enables fast and sustained transcriptional responses to Notch signaling. *Developmental Cell* **50,** 411–425 (2019).

65. Zoller, B., Little, S. C. & Gregor, T. Diverse spatial expression patterns emerge from unified kinetics of transcriptional bursting. *Cell* **175,** 835–847.e25 (2018).

66. Desponds, J. *et al.* Precision of readout at the hunchback gene: analyzing short transcription time traces in living fly embryos. *PLOS Computational Biology* **12** (2016).

67. Lee, C. H., Shin, H. & Kimble, J. Dynamics of Notch-dependent transcriptional bursting in its native context. *Developmental Cell* **50,** 426–435.e4 (2019).

68. Molina, N. *et al.* Stimulus-induced modulation of transcriptional bursting in a single mammalian gene. *Proceedings of the National Academy of Sciences of the United States of America* **110,** 20563–20568 (2013).

69. Rodriguez, J. *et al.* Intrinsic Dynamics of a human gene reveal the basis of expression heterogeneity. *Cell* **176,** 213–226.e18 (2019).

70. Halpern, K. B. Bursty gene expression in the intact mammalian liver. *Molecular Cell* **58,** 147–156 (2015).

71. Suter, D. M. *et al.* Mammalian genes are transcribed with widely different bursting kinetics. *Science* **332,** 472–474 (2011).

72. Tunnacliffe, E., Corrigan, A. M. & Chubb, J. R. Promoter-mediated diversification of transcriptional bursting dynamics following gene duplication. *Proceedings of the National Academy of Sciences of the United States of America* **115,** 8364–8369 (2018).

73. Corrigan, A. M., Tunnacliffe, E., Cannon, D. & Chubb, J. R. A continuum model of transcriptional bursting. *eLife* **5,** e13051 (2016).

74. Gillespie, D. T. Exact stochastic simulation of coupled chemical reactions. *Journal of Physical Chemistry* **81,** 2340–2361 (1977).

75. Lammers, N. C., Kim, Y. J., Zhao, J. & Garcia, H. G. *Code from "A matter of time: Using dynamics and theory to uncover mechanisms of transcriptional bursting"* 2020.

76. Gregor, T., Tank, D. W., Wieschaus, E. F. & Bialek, W. Probing the limits to positional information. *Cell* **130,** 153–164 (2007).

77. Desponds, J., Vergassola, M. & Walczak, A. M. A mechanism for hunchback promoters to readout morphogenetic positional information in less than a minute. *eLife* **9,** e49758 (2020).

78. Schnitzer, M. J. & Block, S. M. Statistical kinetics of processive enzymes. *Cold Spring Harbor Symposia on Quantitative Biology* **60,** 793–802 (1995).

79. Bel, G., Munsky, B. & Nemenman, I. The simplicity of completion time distributions for common complex biochemical processes. *Physical Biology* **7** (2010).